

Effects of La $5d$ and $4f$ states on the electronic and optical properties of LaAlO_3

Jimmy-Xuan Shen,^{1,*} André Schleife,^{2,3} Anderson Janotti,^{4,†} and Chris G. Van de Walle⁴

¹*Department of Physics, University of California, Santa Barbara, California 93106-9530, USA*

²*Condensed Matter and Materials Division, Lawrence Livermore National Laboratory, Livermore, California 94550, USA*

³*Department of Materials Science and Engineering, University of Illinois at Urbana-Champaign, Urbana, Illinois 61801, USA*

⁴*Materials Department, University of California, Santa Barbara, California 93106-5050, USA*

(Received 11 May 2015; revised manuscript received 1 August 2016; published 22 November 2016)

Using first-principles calculations based on density functional theory (DFT) we compare the generalized gradient approximation (GGA-PBE) with a screened hybrid functional by studying the electronic and optical properties of bulk LaAlO_3 in the cubic and rhombohedral phases. We find that both atomic and electronic structures are accurately described by the hybrid functional. The hybrid functional not only corrects the band gap, when compared to GGA-PBE, it also shifts the unoccupied La $4f$ bands to higher energies with respect to the hybridized conduction-band minimum, composed of 83% La $4d$, 5% La $4f$, 6% O $2s$, and 6% O $2p$ states. We show that this shift is essential to accurately describe the complex dielectric function, in good agreement with experimental results. We conclude that the screened hybrid functional offers a reliable description of the position of empty f bands with respect to the valence- and conduction-band edges in LaAlO_3 .

DOI: [10.1103/PhysRevB.94.205203](https://doi.org/10.1103/PhysRevB.94.205203)

I. INTRODUCTION

Lanthanum aluminate, LaAlO_3 or LAO for short, is a wide-band-gap perovskite that is of great interest as a high- k dielectric [1], with reported values of the *static* dielectric constant ranging from 20 to 27 (Refs. [2] and [3]). Bulk LAO offers good lattice matching with many other perovskite materials and is an excellent substrate for epitaxial growth of high- T_c superconductors and magnetic or ferroelectric thin films [4–6]. In complex-oxide heterostructures [7], the combination of LAO with strontium titanate, SrTiO_3 (STO), has been studied extensively due to the formation of a high density two-dimensional electron gas at the interface, even though both materials are conventional band insulators [7].

Despite the great interest in applications, some fundamental properties of bulk LAO are still poorly understood: specifically, the value of the band gap (experimental values range from 5.6 eV to 6.5 eV [8–11]), the position of the La $4f$ states, and the contributions of different orbitals to the optical spectra. First-principles studies have focused on various aspects of LAO and related heterostructures, including electronic properties [12–17], structural phase transitions [18,19], and optical properties [16]. In the isolated La atom, the $4f$ and $5d$ states are close in energy [20]. The electronic configuration of the atom, $[\text{Xe}]6s^25d^1$, actually violates the *Aufbau* principle, which predicts an electronic configuration of $[\text{Xe}]6s^24f^1$. Similarly, in a solid-state environment, the La $4f$ states are usually shifted above the conduction-band edge of the host crystal [21]. Therefore the La $4f$ states have not been discussed in detail [21] or have been outright neglected [22] in first-principles calculations because the band gap is typically given by the transition between O $2p$ and La $5d$ bands. This neglect may be justified from a structural and energetic point of view since the f states are highly localized and do not participate in

bonding. However, the La $4f$ states can play a major role for optical properties. In LAO, they constitute a primary feature in the density of states near the conduction-band edge, and careful consideration of the localized $4f$ states is crucial when calculating and interpreting optical spectra.

Here, we use first-principles methods to determine the electronic and optical properties of LAO in both the cubic phase (c-LAO) and the rhombohedral phase (r-LAO) (see Fig. 1). Calculations of optical spectra for LAO were previously reported in Ref. [16]. However, that study was based on the generalized gradient approximation (GGA), which we will find to be insufficiently accurate. The authors of Ref. [16] also performed an incorrect comparison with experimental data from Ref. [8] (the lower limit of the imaginary dielectric function was misread as 2 instead of 0), affecting the interpretation of their results. We will present a careful comparison with the measured dielectric functions in the literature and focus particular attention on how the description of the localized La $4f$ states affects the computed optical spectra in the vicinity of the absorption onset. This will enable a more accurate interpretation of optical measurements, which can be used to study the charge redistribution at LAO-based interfaces [23]. Ascertaining a more precise value of the band gap will deepen our understanding of the material itself and aid in the design of heterostructures. We also examine the variation in the valence- and conduction-band edges due to the structural changes between c-LAO and r-LAO. Furthermore, our study produces insight regarding the effectiveness of different exchange-correlation functionals in describing the La $4f$ state energies and the optical properties of LAO. These insights should aid future studies of similar materials that combine a strongly polar character and, hence, large static dielectric constant, with strongly localized d and f electrons in the band-edge region.

The paper is organized as follows: In Sec. II, we present the technical aspects of the computational methodology, and in Sec. III, we discuss the results of the structural optimization (Sec. III A) and electronic (Sec. III B) and optical properties (Sec. III C). Section IV concludes the paper.

*jshen@physics.ucsb.edu

†Current address: University of Delaware, Department of Materials Science and Engineering, Newark, DE 19716.

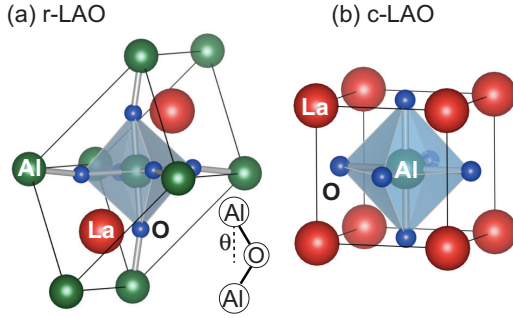


FIG. 1. Crystal structure for (a) rhombohedral LaAlO_3 (r-LAO) and (b) cubic LaAlO_3 (c-LAO). The tilt angle of the octahedra θ is indicated in the inset.

II. COMPUTATIONAL APPROACH

Our calculations are based on density functional theory [24,25] as implemented in the Vienna *ab initio* simulation package (VASP) [26]. To describe exchange and correlation, we use the generalized-gradient approximation (GGA-PBE) of Perdew, Burke, and Ernzerhof [27] as well as the screened hybrid functional of Heyd, Scuseria, and Ernzerhof (HSE06) [28,29]. The exchange-correlation energy in HSE06 is given by

$$E_{XC}^{\text{HSE}} = \frac{1}{4}E_X^{\text{HF,SR}}(\omega) + \frac{3}{4}E_X^{\text{PBE,SR}}(\omega) + E_X^{\text{PBE,LR}}(\omega) + E_C^{\text{PBE}},$$

where the screening parameter ω has the value of 0.2 \AA^{-1} . The mixing ratio of the short-range Hartree-Fock exchange [$E_X^{\text{HF,SR}}(\omega)$] and the long-range PBE exchange [$E_X^{\text{PBE,LR}}(\omega)$] can in principle be used as a tuning parameter. However, for materials with an *electronic* dielectric constant close to 4, the standard 25% mixing is typically a good approximation; additional comments on this issue are included in Sec. III B.

The interactions of valence electrons with the ionic cores are treated through the use of projector augmented wave (PAW) potentials [30]. The La 5s, 5p, 6s, and 5f electrons, the Al 3s and 3p electrons, and the O 2s and 2p electrons are treated as valence electrons. The reciprocal space integration was performed using a mesh of $6 \times 6 \times 6$ special k points following the Monkhorst-Pack scheme [31] for structural optimization of both rhombohedral and cubic phases and

a mesh of $8 \times 8 \times 8$ for the calculation of the frequency-dependent dielectric functions.

The dielectric tensor $\varepsilon^{\alpha\beta}(\omega) = \varepsilon_r^{\alpha\beta}(\omega) + i\varepsilon_i^{\alpha\beta}(\omega)$ is calculated within the PAW framework using the longitudinal approximation [32]. Additional contributions due to excitonic interactions were not considered. From Ref. [32], the imaginary part of the dielectric tensor is given by:

$$\varepsilon_i^{\alpha\beta}(\omega) = \frac{4\pi^2 e^2}{\Omega} \lim_{q \rightarrow 0} \frac{1}{q^2} \sum_{c,v,\mathbf{k}} 2w_{\mathbf{k}} \delta(E_{c\mathbf{k}} - E_{v\mathbf{k}} - \omega) \times \langle u_{c\mathbf{k}+e^\alpha q} | u_{v\mathbf{k}} \rangle \langle u_{v\mathbf{k}} | u_{c\mathbf{k}+e^\beta q} \rangle, \quad (1)$$

where $u_{n\mathbf{k}}$ are the cell-periodic parts of the Bloch wave functions, \mathbf{q} stands for the Bloch vector of the incident beam, and c and v refer to conduction and valence band states, respectively. Since optical excitations are causal, the real part of the dielectric tensor $\varepsilon_r^{\alpha\beta}(\omega)$ can be derived from the imaginary part via Kramers-Kronig relations [33]

$$\varepsilon_r^{\alpha\beta}(\omega) = 1 + \frac{2}{\pi} P \int_0^\infty \frac{\varepsilon_i^{\alpha\beta}(\omega') \omega'}{\omega'^2 + \omega^2 + i\eta} d\omega', \quad (2)$$

where we have used a complex shift of $\eta = 0.1 \text{ eV}$.

III. RESULTS AND DISCUSSION

A. Structural properties

At room temperature, bulk LaAlO_3 has a rhombohedral structure (r-LAO) with space-group symmetry $R\bar{3}c$, containing two formula units in the primitive cell [Fig. 1(a)]. It can be described by the lattice parameter a , representing the length of the three lattice vectors, identical angles $\alpha = \beta = \gamma$ between the three lattice vectors, and an angle θ that represents the rotation of the AlO_6 octahedra. Above 813 K, LAO transitions to a cubic perovskite structure (c-LAO) [34], with one formula unit per primitive cell, characterized by a single lattice parameter a (the length of the three lattice vectors [Fig. 1(b)]). The calculated lattice parameters, compared with experiments and previous calculations, are listed in Table I.

Our GGA-PBE and HSE06 calculations give lattice parameters in good agreement with results from neutron powder diffraction experiments [34] and previous calculations [16,18]. For c-LAO, the agreement between our GGA-PBE lattice parameters with experimental results is misleading because c-LAO is only stable at very high temperatures ($>813 \text{ K}$).

TABLE I. Calculated structural parameters of LaAlO_3 in the rhombohedral (r-LAO) and cubic (c-LAO) phases, including the a and α lattice parameters, and the octahedral tilt angle (θ) for r-LAO. We note that in Ref. [16] and Ref. [18] the authors reported lattice parameters for r-LAO using the conventional cell containing six formula units; we converted these to the values for the primitive cell containing two formula units.

Configuration	Property	GGA-PBE	HSE06	GGA-PBE ^a	GGA-PBE ^b	HSE06 ^b	Exp. ^c
Rhombohedral	a (Å)	5.392	5.342	5.346	5.422	5.381	5.357
	α (°)	60.22	60.20	60.30	60.31	60.20	60.10
	θ (°)	6.3	5.7		4.0	3.1	5.7
Cubic	a (Å)	3.810	3.776		3.830	3.800	3.811

^aReference [16]

^bReference [18]

^cReference [34]

Using a linear expansion coefficient of 2.25×10^{-5} from Ref. [35] to extrapolate the c-LAO lattice parameter to 0 K yields an estimated value of 3.74 Å, which would mean that GGA-PBE overestimates the c-LAO lattice parameter by 1.9%. For r-LAO, GGA-PBE overestimates the lattice parameter a by 0.7% while HSE06 underestimates it by only 0.3%. The tilt angle θ is 6.3° in GGA-PBE and 5.7° in HSE06, compared to the experimental value of 5.7° .

B. Electronic properties

The calculated band structures of c-LAO and r-LAO using GGA-PBE and HSE06 functionals are shown in Fig. 2. The orbital projections of the states in the band structure are also presented: The thickness of the bands represents the magnitude of the projection of the state onto the atomiclike La 4f and 5d orbitals, while the color indicates whether the state has 4f or 5d character. A strongly localized band with exclusively La 4f character is present in each band structure. The state at the conduction-band minimum (CBM) at Γ has predominantly La 5d character in GGA but mixed character in HSE06. The valence-band maximum (VBM) and states further away from the band edges do not exhibit significant contributions from the localized La 4f and La 5d orbitals.

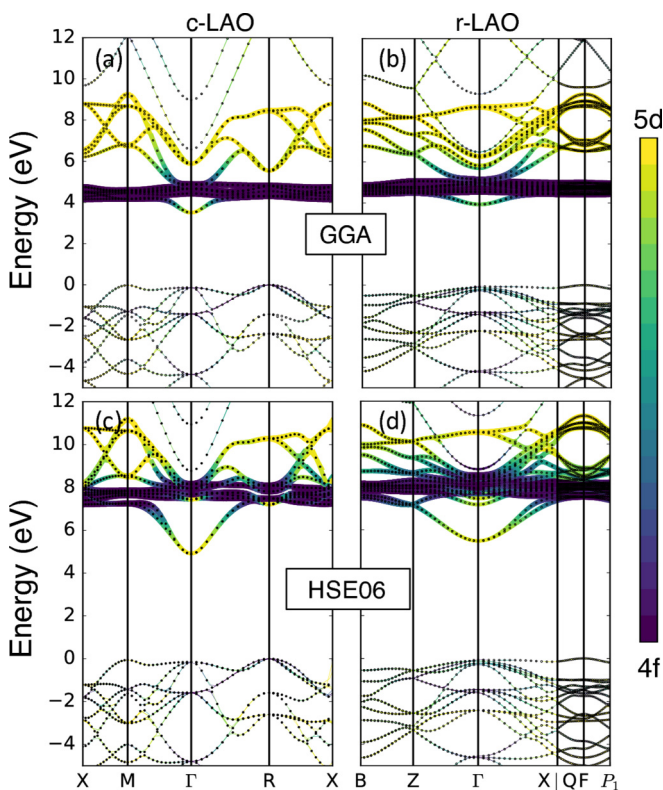


FIG. 2. Band structures of c-LAO in (a) GGA-PBE and (c) HSE06 and band structures of r-LAO in (b) GGA-PBE and (d) HSE06. The valence-band maximum (VBM) was used as the zero-energy reference in each plot. The Kohn-Sham eigenvalues are shown with black or colored dots. The thickness of the bands is proportional to the total projection weights on the 4f and 5d states of La. The color indicates the angular momentum character of the states, according to the color bar on the right.

TABLE II. Calculated band gaps of cubic LaAlO₃ (c-LAO) and rhombohedral LaAlO₃ (r-LAO) phases in GGA-PBE and HSE06. Experimental results from optical ellipsometry and O 1s energy loss spectra are also listed.

Band gap (eV)	Rhombohedral		Cubic	
	Direct	Indirect	Direct	Indirect
GGA-PBE	4.08	4.01	3.61	3.48
HSE06	5.60	5.54	5.04	4.89
Ellipsometry	5.60 ^a	6.33 ^b		
Loss Spectra	6.1 ^c	6.5 ^d		

^aReference [8] — crystalline

^bReference [9] — amorphous

^cReference [10] — crystalline

^dReference [11] — on Si

Independent of the functional, the VBM in c-LAO occurs at R ($\frac{1}{2}, \frac{1}{2}, \frac{1}{2}$) and the CBM at Γ (0,0,0); in r-LAO the VBM is at F ($\frac{1}{2}, \frac{1}{2}, 0$) and the CBM is again at Γ . The indirect and direct band gaps from GGA-PBE and HSE06 calculations are listed in Table II and compared with a range of experimental values from optical ellipsometry [8,9] and O 1s energy loss spectra [10,11]. The band gap derived from energy loss spectra measurements requires linear interpolation of the baseline and loss onset curves, while determination of the band gap using the absorption spectrum from optical ellipsometry does not require any additional numerical interpretation. Thus, the most relevant experimental data comes from the optical ellipsometry measurements of crystalline LAO in Ref. [8].

As expected, comparison to experiment shows that GGA-PBE severely underestimates the band gap. The HSE06 results are much closer to the range of reported experimental values and agree exactly with Ref. [8]. While HSE06 results are not a replacement for quasiparticle energies as calculated within many-body perturbation theory, using for instance Hedin's *GW* approximation [36], it turns out that for many materials the HSE06 results are in good agreement with the experimental values [37,38]. This success, that is attributed to the inclusion of screened exact exchange, can be physically motivated via the similarity of the screened-exchange hybrid functional and the frequency-independent COHSEX approximation of the electronic self energy [39]. From this comparison, it can be seen that one quarter of the Hartree-Fock exchange approximately corresponds to an electronic dielectric constant of 4 that screens the electron-electron interaction. This value agrees very well with the value obtained from our calculations, as reported in Sec. III C.

The band gaps of c-LAO and r-LAO in HSE06 are 1.41 eV and 1.53 eV larger than in GGA-PBE, respectively. Using the HSE06 hybrid functional, the indirect band gap of r-LAO is 0.65 eV larger than that of c-LAO. This is attributed mostly to the narrowing of both the valence band and conduction band in r-LAO due to octahedral distortions: An HSE06 calculation for r-LAO with $\theta = 0^\circ$ yields a band-gap decrease of 0.66 eV, of which 0.22 eV comes from an increase in the VBM and 0.44 eV from a lowering of the CBM. In order to estimate the difference in the position of the VBM in HSE06 with respect to that in GGA-PBE, we performed an HSE06 calculation

for c-LAO strained to the GGA-PBE lattice parameters; since the volumes are now the same, we can assume the averaged electrostatic potentials in HSE06 and GGA-PBE are equal and the band positions are aligned to a common reference. We find that HSE06 lowers the VBM by 1.03 eV and raises the CBM by 0.50 eV with respect to the GGA-PBE values. Repeating the GGA-PBE calculations at the HSE06 lattice parameter produced negligible shifts (<0.1 eV) in the VBM and CBM.

Another striking difference between the band structures in GGA-PBE and HSE06 is the position of the unoccupied La 4*f* bands (cf. Fig. 2). The band structures of both c-LAO and r-LAO exhibit rather flat, localized La 4*f* bands above the CBM. However, the relative energy of the La 4*f* bands changes significantly between GGA-PBE (0.5 eV above the CBM) and HSE06 (2.0 eV above the CBM) calculations, due to the improved description of localized states in HSE06 compared to GGA-PBE. This shows that for this material, the commonly used scissor operator (shifting all of the conduction-band eigenenergies by a fixed amount) will not be sufficient when calculating optical-absorption spectra. While that approach can be used to correct for the band-gap underestimation of GGA-PBE, a correction is also needed for the La 4*f* bands in order to correctly describe optical properties right above the absorption onset (cf. Sec. III C).

The orbital-decomposed densities of states (DOS) for the different atomic species in r-LAO are shown in Fig. 3, along with the total DOS. We find that the CBM is derived from La 5*d* states which extend 6.2 eV above the CBM while the La 4*f* bands are concentrated around a sharp peak 2.2 eV above the CBM. The upper part of the valence band, between -5 eV and 0 eV, is composed predominately of O 2*p* states. Unoccupied Al-related states start at about 2 eV above the CBM and extend to higher energies. We note that in previous HSE06 calculations [18] the La 4*f* bands were not shown, likely because the calculations made use of a localized basis set without *f*-like orbitals.

C. Optical properties

To examine optical properties, we computed the complex frequency-dependent dielectric tensor, given by Eqs. (1) and (2). At low temperatures, only the r-LAO phase is physically relevant for optical measurements, thus, it will be the focus of our optical properties calculations. Although the dielectric function of r-LAO is in principle anisotropic, we find the off-diagonal entries to be negligible, and the diagonal entries are nearly identical. Hence, we only report the average of the three diagonal components of the dielectric tensor. The real part $\epsilon_r(\omega)$ and the imaginary part $\epsilon_i(\omega)$ are plotted in Fig. 4.

The imaginary part of the dielectric function, calculated in HSE06, exhibits two peaks, at 8.32 eV and 9.69 eV. By projecting the conduction-band states in Eq. (1) onto distinct atomic orbitals, we can estimate the contributions to the imaginary dielectric function from the various atomic states [see Fig. 4(a)]. At the photon energy of the first peak ($\omega = 8.32$ eV), the contributions to the imaginary dielectric function come primarily from optical transitions to La-*d* (29%) and La-*f* (65%). The contributions to the second peak ($\omega = 9.69$ eV) are also primarily from the same orbitals, with

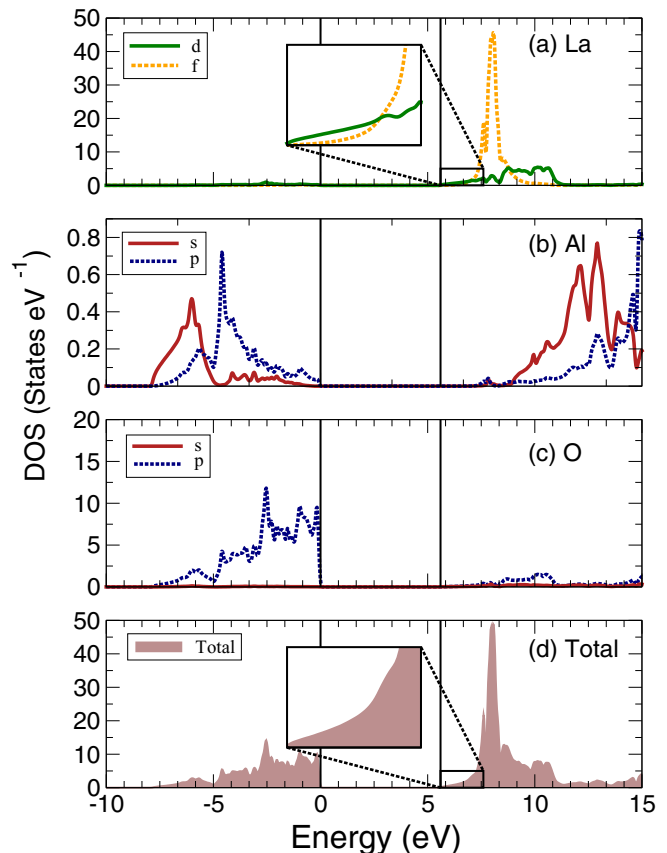


FIG. 3. Orbital-decomposed density of states (DOS) for r-LAO calculated in HSE06 for each atomic species. The highest two orbital contributions of the atom-projected DOS are shown for (a) La, (b) Al, and (c) O. The total DOS for r-LAO is shaded gray in (d), and VBM and CBM are indicated by vertical lines. The insets show the bottom of the conduction band (5.6–7.6 eV); contributions from the Al and O orbitals are negligible in this range.

38% attributed to the La-*d* orbitals and 50% attributed to the La-*f* orbitals. Since states with high angular momentum account for the majority of contributions to these two peaks, an accurate approach to describe the energy and momentum dependence of localized states is necessary in order to compute reliable optical spectra. The prominent role of *f* states near the band edge justifies our choice to use the HSE06 functional, which is known to accurately describe strongly localized states.

In comparing the calculated spectra with experiment, it is important to understand the limitations in the accuracy of the experiments. In the study by Asmara *et al.* [23] (“Exp.^b” in Fig. 4), the dielectric functions of LAO were obtained using a combination of spectroscopic ellipsometry (in the energy range 0.5–5.6 eV) and reflectivity (3.7–35 eV) measurements. Because the ellipsometry data is more reliable, the reflectivity data was renormalized to match the ellipsometry data in that energy range. However, the entire range of energies for the ellipsometry measurements is below the direct gap of r-LAO (5.60 eV), and thus there is no reference peak available in that range, making the overall scaling of the reported spectra unreliable. For the measurement reported in Ref. [8] (“Exp.^a”), the authors used spectroscopic ellipsometry over the entire experimental energy range (4.8–9.0 eV). We note that in the

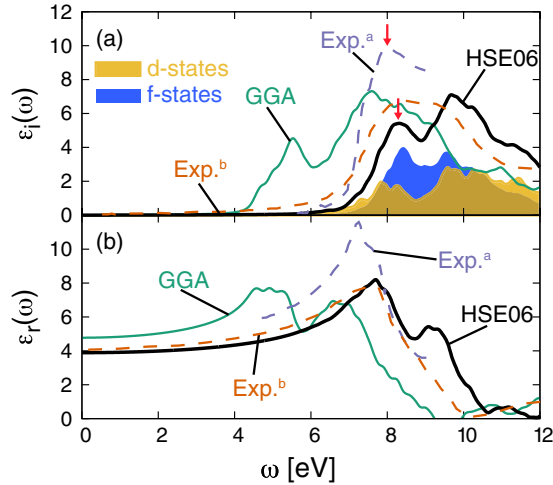


FIG. 4. (a) Imaginary and (b) real components of the dielectric function for r-LAO. Results of the GGA-PBE (green) and HSE06 (black) calculations are shown and compared with Exp.^a (from Fig. 4 in Ref. [8]) and Exp.^b (from Fig. 5 in Ref. [23]). The contribution to the HSE06 imaginary dielectric function due to transitions to *d* and *f* states in the conduction band are also shown. Arrows indicate the first peak in the imaginary dielectric function which we attribute to transitions involving the La 4*f* states.

energy range 4.8–5.6 eV, where both experimental studies report ellipsometry measurements, the dielectric function still differs in absolute amplitude between the two studies. We are led to conclude that the amplitudes of the reported spectra depend on the exact procedure used to obtain them. The absolute amplitude should thus not be a focal point in the comparison of our calculated spectra with experiments, and we will primarily focus on the onset and peak positions of the imaginary dielectric function.

Figure 4 shows that the shape and the onset of the HSE06 dielectric function is very similar to those observed in experiments [8,23], lending confidence to our comparison of the calculated band gaps in HSE06 with experimental results in Table II. The position and onset of the first peak in the measured imaginary dielectric function match the La 4*f* peak in our HSE06 calculations, allowing us to attribute the primary peak in Ref. [8] to transitions between the valence band and 5*d*/4*f* states in the conduction band.

As to the comparison of the HSE06 and GGA-PBE calculations, the difference is particularly evident in the shape and position of the first peak. This is mainly due to the difference in the position of the La 4*f* bands relative to the CBM, as discussed above. The pronounced shift of *f* bands to higher energies in HSE06 causes the two main peaks in the spectrum to be closer to each other in HSE06 (at 8.32 eV and 9.69 eV) than in GGA-PBE (5.53 eV and 7.59 eV). One may wonder why this double-peak feature, prominent in the calculated spectra, is not evident in the experimental dielectric functions. With regard to Ref. [8] (“Exp.^a”), the reason is that the reported energy range barely extends beyond the first peak. For Ref. [23] (“Exp.^b”), the dielectric functions are obtained via a self-consistent iterative scheme from the reflectivity, which introduces uncertainties, as discussed below. We note that the original reflectivity data

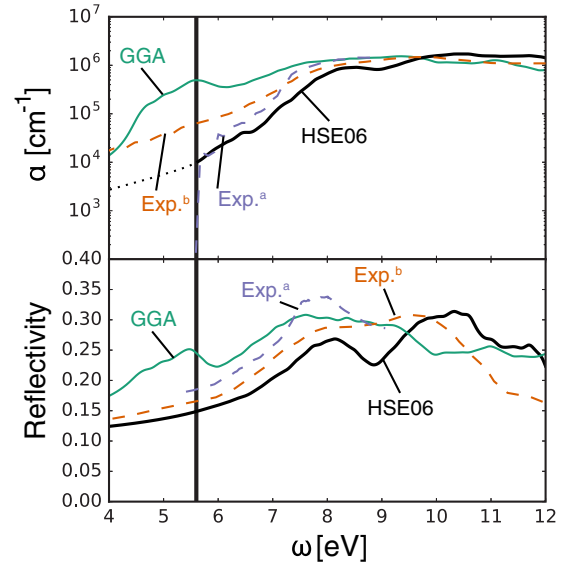


FIG. 5. (a) Frequency-dependent absorption coefficient and (b) optical reflectivity of r-LAO. Results of the GGA-PBE (green) and HSE06 (black) calculations are shown and compared with experiments (Exp.^a, digitized from Fig. 5 in Ref. [8] and Exp.^b, digitized from Fig. 2.c in Ref. [23]). The finite absorption coefficients at energies below the band gap for HSE06 (indicated by a vertical line) are an artefact of the energy smearing, as discussed in the text, and indicated with a dotted line.

does exhibit two clear shoulders, mirroring the two peaks in the HSE06 reflectivity spectrum [see Fig. 5(b)].

We also highlight that the computed value of the *electronic* dielectric constant ($\epsilon_r = 3.9$ at low frequencies) agrees very well with the experimental result of Ref. [23]. This electronic dielectric constant (sometimes also called “high-frequency” dielectric constant) is different from the *static* dielectric constant which includes the lattice response and is reported to be between 20 and 27 (Refs. [2] and [3]).

Additional optical properties can be derived from the real and imaginary parts of the dielectric functions [40]. The absorption coefficient α is given by

$$\alpha(\omega) = \frac{\sqrt{2}\omega}{c} \left(\sqrt{\epsilon_r^2 + \epsilon_i^2} - \epsilon_r \right)^{\frac{1}{2}}, \quad (3)$$

and the optical reflectivity R by

$$R(\omega) = \frac{(n(\omega) - 1)^2 + \kappa(\omega)^2}{(n(\omega) + 1)^2 + \kappa(\omega)^2}, \quad (4)$$

where n and κ are the components of the complex refractive index given by

$$n = \sqrt{\frac{|\epsilon_r + i\epsilon_i| + \epsilon_r}{2}} \quad \text{and} \quad \kappa = \sqrt{\frac{|\epsilon_r + i\epsilon_i| - \epsilon_r}{2}}. \quad (5)$$

The experimental absorption coefficient α was reported explicitly in Ref. [8], and we used Eq. (3) to compute the absorption coefficient from ϵ_r and ϵ_i extracted from Fig. 5 of Ref. [23]. For small values of ϵ_i the absorption coefficient follows from $\alpha \approx \omega\epsilon_i/(c\sqrt{\epsilon_r})$. The real part of the dielectric function remains finite below the band gap. Hence, the absorption

spectrum must vanish along with the imaginary dielectric function. This is indeed evident in the data from Ref. [8], which exhibits a sharp drop in the absorption coefficient below the band gap of LAO [Fig. 5(a)].

The small- ε_i expansion of the reflectivity contains a nonzero term that is independent of ε_i . Due to this leading ε_i -independent term, the reflectivity spectrum is not sensitive to changes in ε_i that are small on an absolute scale but substantial relative to the small values of ε_i near and below the band gap. Specifically, the self-consistent iteration procedure used in Ref. [23] to obtain the dielectric functions from the measured reflectivity spectrum can result in a ε_i spectrum with nonvanishing ε_i values below the gap (where ε_i should be uniformly zero). While the reflectivity spectrum is insensitive to ε_i near and below the band gap, the absorption spectrum is linearly dependent on ε_i . This explains why the absorption spectrum derived using the dielectric functions from Ref. [23] differs greatly from the ellipsometry results of Ref. [8] and from our calculations, particularly near and below the band gap when $\varepsilon_i \ll 1$.

The calculated results for the absorption spectrum and reflectivity are also shown in Fig. 5. HSE06 results are again in much better agreement with experiment than GGA-PBE results, due to the improved descriptions of the band gap and La 4*f* states. Figure 5(a) illustrates that agreement with the experimental data for the absorption coefficient is good for values above the band gap. However, the steep drop in absorption that we expect to see below the band gap (which is evident in the directly measured spectra from Ref. [8], and indeed used to identify the band gap) does not occur in the calculated spectra. The calculated absorption spectrum suffers from a problem similar to that mentioned in the context of extracting the data from Ref. [23]: While the calculated imaginary dielectric function ε_i is very small below the band gap, it is not exactly zero and there is a continuous tail that extends well below the band-gap energy. This is an artifact of the use of smearing, which is required to replace the δ function in Eq. (1) when summing over a finite set of discrete k points. These calculated absorption spectra are therefore useful to compare with experiment at values above the gap but should not be used to determine the value of the band gap; the calculated results for the band structure are of course much better suited to that purpose.

The HSE06 results for reflectivity [Fig. 5(b)] also show good agreement with direct measurements from Ref. [23]. Notably, the onset position of the first peak in the HSE06 results and the leading shoulder of the measured reflectivity fall within 0.2 eV. The agreement is much better than for the GGA-PBE results which can, again, be attributed

to a more accurate band gap and a better description of the separation between the CBM and the La 4*f* derived states.

IV. CONCLUSIONS

In conclusion, we have performed first-principles calculations for the electronic structure and optical properties of LAO. Results obtained with the HSE06 functional offer significant improvements over those obtained with GGA-PBE, most notably for the band gap and the position of the empty La 4*f* bands. HSE06 predicts a direct band gap of 5.60 for r-LAO (0.06 eV larger than the indirect gap). This value matches with what we believe is the most accurate experimental determination [8]. The HSE06 calculations show that the unoccupied La 4*f* bands are much higher in energy with respect to the CBM, compared with GGA-PBE calculations. This shows that the commonly used scissor approach is unreliable for LAO, and we expect the same to be true for other materials with localized *d* and *f* states. The improved description of this peak in HSE06, along with a more accurate value of the band gap, allows us to calculate the optical spectra of LAO with improved accuracy. A double-peak structure is observed in the optical imaginary dielectric function and the reflectivity spectrum. By separating the contributions from La 4*f* and 5*d* states in the conduction band, we can attribute the first peak predominantly to transition involving La 4*f* states. We also demonstrated that for physically relevant observables such as the absorption spectrum and reflectivity, HSE06 not only produces the correct onset (due to a better prediction of the band gap) but also an overall shape of the spectra in much better agreement with the best available experimental data. Experiments aimed at more accurately measuring the dielectric function and using larger photon energies are called for.

ACKNOWLEDGMENTS

This work was supported by the Center for Low Energy Systems Technology (LEAST), one of six SRC STARnet Centers sponsored by MARCO and DARPA, and by the NSF MRSEC program (DMR-1121053). Part of this work was performed under the auspices of the U.S. Department of Energy at Lawrence Livermore National Laboratory under Contract DE-AC52-07A27344. Computational resources were provided by the Center for Scientific Computing at the CNSI and MRL (an NSF MRSEC, DMR-1121053) (NSF CNS-0960316), and by the Extreme Science and Engineering Discovery Environment (XSEDE), supported by NSF (ACI-1053575).

[1] J. A. Kittl, K. Opsomer, M. Popovici, N. Menou, B. Kaczer, X. P. Wang, C. Adelman, M. A. Pawlak, K. Tomida, A. Rothschild, B. Govoreanu, R. Degraeve, M. Schaekers, M. Zahid, A. Delabie, J. Meererschaut, W. Polspoel, S. Clima, G. Pourtois, W. Knaepen, C. Detavernier, V. Afanas'ev, T. Blomberg, D. Pierreux, J. Swerts, P. Fischer, J. W. Maes, D.

Manger, W. Vandervorst, T. Conrad, A. Franquet, P. Favia, H. Bender, B. Brijs, S. V. Elshocht, M. Jurczak, J. V. Houdt, and D. J. Wouters, *ECS Trans.* **19**, 29 (2009).

[2] B.-E. Park and H. Ishiura, *Appl. Phys. Lett.* **82**, 1197 (2003).

[3] X.-b. Lu, Z.-g. Liu, Y.-p. Wang, Y. Yang, X.-p. Wang, H.-w. Zhou, and B.-y. Nguyen, *J. Appl. Phys.* **94**, 1229 (2003).

- [4] S. Gariglio, N. Reyren, A. D. Caviglia, and J.-M. Triscone, *J. Phys.: Condens. Matter* **21**, 164213 (2009).
- [5] M. Ben Shalom, M. Sachs, D. Rakhmilevitch, A. Palevski, and Y. Dagan, *Phys. Rev. Lett.* **104**, 126802 (2010).
- [6] J. A. Bert, B. Kalisky, C. Bell, M. Kim, Y. Hikita, H. Y. Hwang, and K. A. Moler, *Nat. Phys.* **7**, 767 (2011).
- [7] A. Ohtomo and H. Y. Hwang, *Nature (London)* **427**, 423 (2004).
- [8] S.-G. Lim, S. Kriventsov, T. N. Jackson, J. H. Haeni, D. G. Schlom, A. M. Balbashov, R. Uecker, P. Reiche, J. L. Freeouf, and G. Lucovsky, *J. Appl. Phys.* **91**, 4500 (2002).
- [9] E. Cicerrella, J. Freeouf, L. Edge, D. Schlom, T. Heeg, J. Schubert, and S. A. Chambers, *J. Vac. Sci. Technol. A* **23**, 1676 (2005).
- [10] Z. Liu, W. Chim, S. Chiam, J. Pan, and C. Ng, *Thin Solid Films* **534**, 177 (2013).
- [11] Y. Y. Mi, Z. Yu, S. J. Wang, P. C. Lim, Y. L. Foo, A. C. H. Huan, and C. K. Ong, *Appl. Phys. Lett.* **90**, 181925 (2007).
- [12] R. Pentcheva and W. E. Pickett, *Phys. Rev. Lett.* **102**, 107602 (2009).
- [13] H. Chen, A. M. Kolpak, and S. Ismail-Beigi, *Phys. Rev. B* **79**, 161402 (2009).
- [14] A. A. Knizhnik, I. M. Iskandarova, A. A. Bagatur'yants, B. V. Potapkin, L. R. C. Fonseca, and A. Korkin, *Phys. Rev. B* **72**, 235329 (2005).
- [15] M. Choi, A. Janotti, and C. G. Van de Walle, *Phys. Rev. B* **88**, 214117 (2013).
- [16] X. Luo and B. Wang, *J. Appl. Phys.* **104**, 053503 (2008).
- [17] A. Janotti, L. Bjaalie, L. Gordon, and C. G. Van de Walle, *Phys. Rev. B* **86**, 241108 (2012).
- [18] F. El-Mellouhi, E. N. Brothers, M. J. Lucero, I. W. Bulik, and G. E. Scuseria, *Phys. Rev. B* **87**, 035107 (2013).
- [19] C. J. Först, K. Schwarz, and P. E. Blöchl, *Phys. Rev. Lett.* **95**, 137602 (2005).
- [20] J. M. Mariot, R. C. Karnatak, H. Search, C. Journals, A. Contact, M. Iopscience, and I. P. Address, *J. Phys. F* **4**, L223 (1974).
- [21] J. He and C. Franchini, *Phys. Rev. B* **86**, 235117 (2012).
- [22] F. El-Mellouhi, E. N. Brothers, M. J. Lucero, and G. E. Scuseria, *Phys. Rev. B* **88**, 214102 (2013).
- [23] T. C. Asmara, A. Annadi, I. Santoso, P. K. Gogoi, A. Kotlov, H. M. Omer, M. Motapothula, M. B. H. Breese, M. Rübhausen, T. Venkatesan, Ariando, and A. Rusydi, *Nat. Commun.* **5**, 4663 (2014).
- [24] W. Kohn and L. J. Sham, *Phys. Rev.* **140**, A1133 (1965).
- [25] P. Hohenberg and W. Kohn, *Phys. Rev.* **136**, B864 (1964).
- [26] G. Kresse and D. Joubert, *Phys. Rev. B* **59**, 1758 (1999).
- [27] J. P. Perdew, K. Burke, and M. Ernzerhof, *Phys. Rev. Lett.* **78**, 1396 (1997).
- [28] J. Heyd, G. E. Scuseria, and M. Ernzerhof, *J. Chem. Phys.* **118**, 8207 (2003).
- [29] J. Heyd, G. E. Scuseria, and M. Ernzerhof, *J. Chem. Phys.* **124**, 219906 (2006).
- [30] P. E. Blöchl, *Phys. Rev. B* **50**, 17953 (1994).
- [31] H. J. Monkhorst and J. D. Pack, *Phys. Rev. B* **13**, 5188 (1976).
- [32] M. Gajdoš, K. Hummer, G. Kresse, J. Furthmüller, and F. Bechstedt, *Phys. Rev. B* **73**, 045112 (2006).
- [33] J. S. Toll, *Phys. Rev.* **104**, 1760 (1956).
- [34] S. A. Hayward, F. D. Morrison, S. A. T. Redfern, E. K. H. Salje, J. F. Scott, K. S. Knight, S. Tarantino, A. M. Glazer, V. Shuvaeva, P. Daniel, M. Zhang, and M. A. Carpenter, *Phys. Rev. B* **72**, 054110 (2005).
- [35] B. C. Chakoumakos, D. G. Schlom, M. Urbanik, and J. Luine, *J. Appl. Phys.* **83**, 1979 (1998).
- [36] L. Hedin, *Phys. Rev.* **139**, A796 (1965).
- [37] M. Marsman, J. Paier, A. Stroppa, and G. Kresse, *J. Phys.: Condens. Matter* **20**, 064201 (2008).
- [38] A. Janotti, J. B. Varley, P. Rinke, N. Umezawa, G. Kresse, and C. G. Van de Walle, *Phys. Rev. B* **81**, 085212 (2010).
- [39] A. Alkauskas, P. Broqvist, and A. Pasquarello, *Phys. Status Solidi B* **248**, 775 (2011).
- [40] G. Grosso and P. Parravicini, *Solid State Physics*, 2nd ed. (Elsevier, Oxford, UK, 2014).